

2021

## The Role of Dynamic Wetting Behavior during Bubble Growth and Departure from a Solid Surface

Taylor P. Allred  
*Purdue University*, allredt@purdue.edu

Justin A. Weibel  
*Purdue University*, jaweibel@purdue.edu

S V. Garimella  
*Purdue Univ*, sureshg@purdue.edu

Follow this and additional works at: <https://docs.lib.purdue.edu/coolingpubs>

---

Allred, Taylor P.; Weibel, Justin A.; and Garimella, S V., "The Role of Dynamic Wetting Behavior during Bubble Growth and Departure from a Solid Surface" (2021). *CTRC Research Publications*. Paper 378. <http://dx.doi.org/10.1016/j.ijheatmasstransfer.2021.121167>

This document has been made available through Purdue e-Pubs, a service of the Purdue University Libraries. Please contact [epubs@purdue.edu](mailto:epubs@purdue.edu) for additional information.

# The Role of Dynamic Wetting Behavior during Bubble Growth and Departure from a Solid Surface<sup>1</sup>

Taylor P. Allred<sup>2</sup>, Justin A. Weibel<sup>3</sup>, Suresh V. Garimella<sup>4</sup>  
School of Mechanical Engineering and Birck Nanotechnology  
Purdue University, West Lafayette, IN 47907

## ABSTRACT

Surface wettability is known to have a major influence on the ebullition characteristics of a bubble growing from a solid surface. Yet, simplistic static characterization of the wetting behavior is still relied upon to indicate performance characteristics during boiling. In this study, a theoretical framework is developed for the wetting and dewetting processes occurring during bubble growth based upon the dynamic contact angles. This framework is incorporated into adiabatic volume-of-fluid simulations to capture the influence of the surface wettability on contact line and contact angle dynamics during bubble growth and departure. The simulations span a large range of dynamic wetting behaviors and fluid properties. The receding contact angle is shown to govern the early stages of bubble growth as the contact line recedes outward from the bubble center and is the dominant wetting characteristic that determines the maximum contact diameter and departure size. The advancing contact angle dictates the departure morphology as the contact line retracts inward and has a secondary role in determining the

---

<sup>1</sup> Submitted for possible publication in *International Journal of Heat and Mass Transfer*.

<sup>2</sup> E-mail address: tallred11@gmail.com.

<sup>3</sup> E-mail address: jaweibel@purdue.edu.

<sup>4</sup> Corresponding author, currently President, University of Vermont. Tel.: +1 802 656 7878. E-mail address: sureshg@purdue.edu.

departure size. Following, improved reduced-order models are developed that establish fluid-property-independent correlations for the maximum contact diameter and departure diameter as a function of the dynamic contact angles. The results call for the need to redefine wettability classifications based on dynamic contact angles rather than static contact angle in the context of boiling. Hygrophilicity and hygrophobicity are redefined in this context, and an additional classification, ambiphilicity, is introduced for boiling surfaces exhibiting low receding contact angles and high advancing contact angles.

**Keywords:** bubble growth, bubble departure, contact lines, multiphase flow, phase change, boiling, dynamic wetting

## 1. INTRODUCTION

Proper understanding of the bubble dynamics during boiling is critical to achieving effective and predictable heat transfer in applications such as refrigeration, distillation, and high-density cooling of nuclear reactors and power electronics. Changes in the bubble morphology and contact line dynamics are known to have a substantial impact on transport during boiling processes. Ebullition characteristics such as the bubble departure diameter, departure frequency, and growth rate are widely studied<sup>1,2</sup> due to their governing role in heat transfer and hydrodynamics. For the vast majority of applications featuring heterogeneous bubble nucleation that occurs at a solid surface, the wettability of the surface is known to dictate bubble morphology throughout the ebullition cycle<sup>3-8</sup>.

Surface wettability is commonly characterized by the contact angle<sup>9</sup> measured from the solid-liquid interface to the liquid-vapor interface at the three-phase contact line of a droplet viewed from the side. On an ideal, smooth surface, the contact angle is defined as the equilibrium contact angle given by Young's equation<sup>10</sup>,  $\gamma_{lv} \cos \theta_E = \gamma_{sv} - \gamma_{sl}$ , where  $\gamma_{lv}$  is the liquid-vapor interfacial tension,  $\gamma_{sv}$  the solid-vapor interfacial tension,  $\gamma_{sl}$  the solid-liquid interfacial tension, and  $\theta_E$  the equilibrium contact angle. For real surfaces, there are three contact angles that are considered: static, advancing, and receding. The static contact angle,  $\theta_{static}$ , measured for a sessile droplet resting on a horizontal surface as shown in figure 1(a), is the most commonly reported wettability metric in studies on boiling. The static contact angle is often erroneously considered as a proxy for the equilibrium contact angle, but this is only an appropriate assumption in cases where the contact angle hysteresis (difference between the advancing and receding contact angles) is very low<sup>9</sup>. The static contact angle can manifest as any angle between the advancing and receding contact angle, depending on the droplet history (*e.g.*, deposition method,

evaporation, etc.), and it is therefore an inexact measure for the majority of real surfaces which have appreciable contact angle hysteresis<sup>11</sup>. The advancing ( $\theta_{adv}$ ) and receding ( $\theta_{rec}$ ) contact angles are measured during motion of the three-phase contact line. For example, for a droplet sliding on a tilted surface, as illustrated in figure 1(b), the advancing contact angle can be measured at the leading edge of the droplet and the receding contact angle at the trailing edge. Dynamic contact angles can alternatively be measured by inserting a small needle into the droplet and adding or removing liquid until the contact line begins to move. These dynamic contact angles are indicative of the unique contact line behavior on a surface and are not dependent on droplet history, permitting consistent measurement regardless of the contact angle hysteresis.

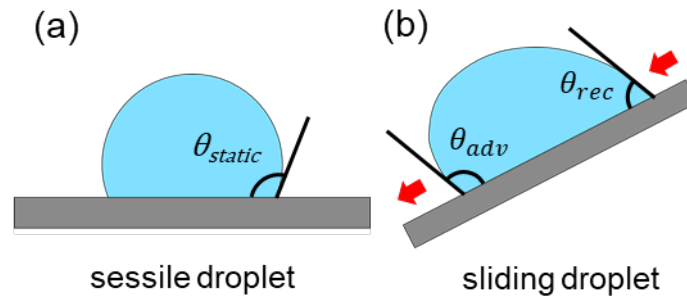


**Figure 1.** Schematic illustrations of (a) the static contact angle measured for a sessile droplet on a surface and (b) the dynamic advancing and receding contact angles measured for a sliding droplet.

In the context of bubble dynamics during departure from a solid surface, studies that incorporate the effect of surface wettability are often limited to static contact angle characterizations. The seminal Fritz correlation<sup>12</sup> for bubble departure diameter, given as

$$D_d = 0.0208\theta_{static}\sqrt{2\sigma / g(\rho_l - \rho_v)},$$

predicts that the departure diameter increases linearly with

static contact angle. Most extant studies regarding the effect of surface wettability on boiling behavior only characterize the static contact angle and correlate changes in the boiling behavior with differences in the static contact angle<sup>4,6,13-17</sup>. Notionally hydrophilic surfaces characterized by static contact angles with water of less than 90 deg are observed to have relatively small, rapidly departing bubbles. Notionally hydrophobic surfaces characterized by static contact angles with water greater than 90 deg are observed to have large bubbles that tend to spread over the surface and remain attached for extended periods of time. This simplistic approach of describing wetting behavior during boiling with static characterizations offers an adequate, yet imprecise, understanding of the role of wettability, but only for surfaces having relatively low contact angle hysteresis. However, this approach severely misrepresents the role of surface wettability on boiling for surfaces with high contact angle hysteresis. For example, recent reports of bubble dynamics on certain textured hydrophobic surfaces do not follow the expected trends based on static contact angle<sup>8,18,19</sup>.

Superhydrophobic surfaces are commonly known for having high static contact angles and low contact angle hysteresis. This behavior is exhibited when the liquid rests on top of a surface texture in the Cassie-Baxter wetting state, minimizing liquid-solid contact<sup>20</sup>. However, the Cassie-Baxter state is typically metastable, and if disturbed, the liquid can transition into the Wenzel wetting state by penetrating into the surface texture<sup>21</sup>. In contrast to the Cassie-Baxter state, very high contact angle hysteresis is observed in the Wenzel state<sup>22</sup>. The authors have recently demonstrated that superhydrophobic surfaces display contrasting bubble dynamics depending on whether the surface is initially primed to have liquid in the Cassie-Baxter wetting state or the Wenzel wetting state<sup>19</sup>. Large bubbles spread over large portions of the surface when the liquid is in the Cassie-Baxter state, as expected based on the trends established using static

characterizations. However, very small bubbles with pinned contact diameters grow from the surface when the liquid is in the Wenzel state despite the surface possessing a high static contact angle. Additionally, the authors have shown that parahydrophobic surfaces, which exhibit very high contact angle hysteresis, generate small vapor bubbles during boiling despite having high static contact angles<sup>8</sup>. These findings contradict the current understanding of the effect of surface wettability on bubble dynamics during boiling that has been established based on flawed static contact angle characterizations. The dynamic wetting behavior, which has been shown to play an important role in other phase change processes such as condensation<sup>23–27</sup> and droplet evaporation<sup>28–32</sup>, must be taken into account to correlate boiling characteristics to surface wettability due to their role in contact line dynamics.

While several studies have observed the dynamic contact angle evolution during bubble growth<sup>8,33–35</sup>, the effect of these dynamic contact angles has not been adequately incorporated into models for bubble ebullition. Some bubble departure models have been developed that solely include either the advancing<sup>36</sup> or receding contact angle<sup>8</sup>, but not both. Mukherjee and Kandlikar<sup>37</sup> performed single bubble growth simulations that incorporated dynamic contact angles, but only considered hydrophilic surfaces having a small range of dynamic contact angles. Chen *et al.*<sup>38</sup> performed simulations of single bubble growth from an orifice plate and considered a wide range of dynamic contact angles, but the conclusions drawn regarding the effects of advancing and receding contact angles on bubble morphology are not directly applicable to bubble growth during boiling due to the orifice dictating the contact diameter during portions of the ebullition cycle.

The current study seeks to develop a comprehensive understanding of the roles of both the advancing and receding contact angles during bubble growth from a solid surface. This

understanding is incorporated into readily usable models that accurately predict ebullition characteristics. First, a basic theoretical framework for bubble growth is proposed based upon fundamental wetting and dewetting processes that occur on a solid surface. This dynamic wetting framework is incorporated into numerical simulations that examine the effect of differing receding and advancing contact angles on bubble growth and departure morphologies. The numerical results are compared against experiments, and fluid-property-independent correlations are extracted for the maximum contact diameter and bubble departure diameter.

## 2. METHODS

### 2.1 Theoretical Framework for Dynamic Wetting during Bubble Growth and Departure

We propose an intuitive framework for the contact angle and contact line dynamics during bubble growth that is based on well-established fundamental wetting dynamics<sup>9</sup>. The key assertion is that contact line motion (or lack thereof) is governed by the dynamic contact angles. If the liquid is at the receding contact angle, the contact line can recede (dewetting) if the forces acting so dictate, but it cannot advance. Similarly, the contact line can only advance (wetting) when the liquid is at the advancing contact angle. At any contact angle between the advancing and receding contact angles, the contact line will be pinned in place; instead of inducing contact line motion, any forces acting in this state will alter the contact angle and bubble morphology.

When discussing the proposed framework for bubble growth and departure, the contact angles referenced are always with respect to the liquid. The dominant forces considered during quasi-steady growth are the buoyant force ( $F_b = (\rho_l - \rho_v)Vg$ , where  $\rho_l$  is the liquid density,  $\rho_v$  the vapor density,  $V$  the bubble volume, and  $g$  the gravitational acceleration), and the vertical component of the surface tension force ( $F_s = \sigma\pi D_c \sin \theta$ , where  $\sigma$  is the surface tension,  $D_c$  the

contact diameter, and  $\theta$  the instantaneous contact angle). During the initial stage of bubble growth, the receding stage, the contact line expands from the nucleation site as the bubble grows (*i.e.*, the liquid recedes from the nucleation site), as shown in figure 2(a). During this dewetting process, the liquid is at the receding contact angle. Eventually, a critical force balance is reached where the surface tension forces can no longer compensate for the increasing buoyant forces at the receding contact angle. Because the bubble is still at the receding contact angle at this instant, the contact line will not yet advance to depart, as it can only advance at the *advancing* contact angle. Instead, during the pinning stage, the contact line will remain pinned in place, as shown in figure 2(b), while the contact angle will begin to increase to accommodate the increasing buoyant force acting on the growing bubble. Once the bubble has grown such that the advancing contact angle is reached, the advancing stage begins and the liquid can rewet the surfaces as the contact line advances at the advancing contact angle, as shown in figure 2(c). To summarize, the bubble initially grows in a constant contact angle mode at the receding contact angle during the receding stage, followed by a constant contact radius mode as the contact angle increases over the span of contact angle hysteresis in the pinning stage, and finally a constant contact angle mode at the advancing contact angle in the advancing stage. Kim *et al.*<sup>35</sup> reported a similar three-stage process based on experimental measurements and attributed the transitions between stages to differences in free energy rather than the dynamic contact angles. The resulting dynamics are analogous to those commonly reported for droplet evaporation featuring constant contact radius and constant contact angle modes<sup>28</sup>.

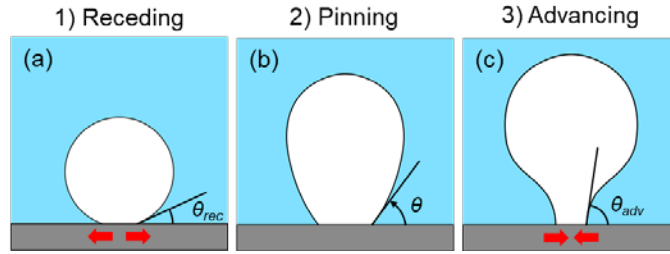


**Figure 2.** Illustration of the wetting dynamics during bubble growth: (a) the receding stage during which the contact line dewets the surface at the receding contact angle; (b) the pinning stage during which the contact angle increases while there is no contact line motion; and (c) the advancing stage during which the contact line rewets the surface at the advancing contact angle.

Following this framework, the bubble morphology during growth and departure is governed by the dynamic contact angles; the static contact angle need not be considered as it has no role in contact line or contact angle dynamics. The bubble morphology during the early stages of growth is governed by the receding contact angle, and the departure morphology is governed by the advancing contact angle. For this analysis, the growth is assumed to be quasi-steady and dominated by surface tension and buoyancy effects. Accordingly, the effect of contact line velocity on the dynamic contact angles is neglected, though it may have an influence during rapid bubble growth<sup>11,39</sup>.

## 2.2 Numerical Simulation of Bubble Growth and Departure with Dynamic Wetting Effects

The framework for the contact line and contact angle dynamics during bubble growth and departure is implemented within a transient, two-phase, continuum surface force volume-of-fluid (CSF-VOF) simulation (ANSYS Fluent<sup>40</sup>) to determine the roles of the advancing and receding contact angles on the bubble morphology, departure diameter, and maximum contact diameter. For a discussion regarding the impact of the assumptions used in developing these simulations

and their applicability to boiling situations, please refer to Section 3.5. The simulations are performed using a rectangular, 2D axisymmetric domain as shown in figure 3. A uniform square mesh with cell widths of 0.01 mm is applied throughout the domain. This mesh size provides a minimum of 30 cells across the radius of curvature of any bubble in the study and is expected to provide sufficient mesh size independence. The domain size is adjusted for each case based on the bubble size to minimize computational time while avoiding interactions with the side walls. Because of the quasisteady nature of the simulations, the velocities in the liquid are low and no impactful interactions between the bubble and the side wall were observed. The top boundary acts as an outlet at a constant pressure of 1 atm. The outer radial boundary is a no-slip wall. A user-defined boundary condition for the contact angle and contact line of the bubble is applied to the bottom boundary based on the proposed dynamic wetting framework. The simulation is adiabatic and bubble growth occurs through addition of mass to the vapor region; no heat transfer or phase change is considered.

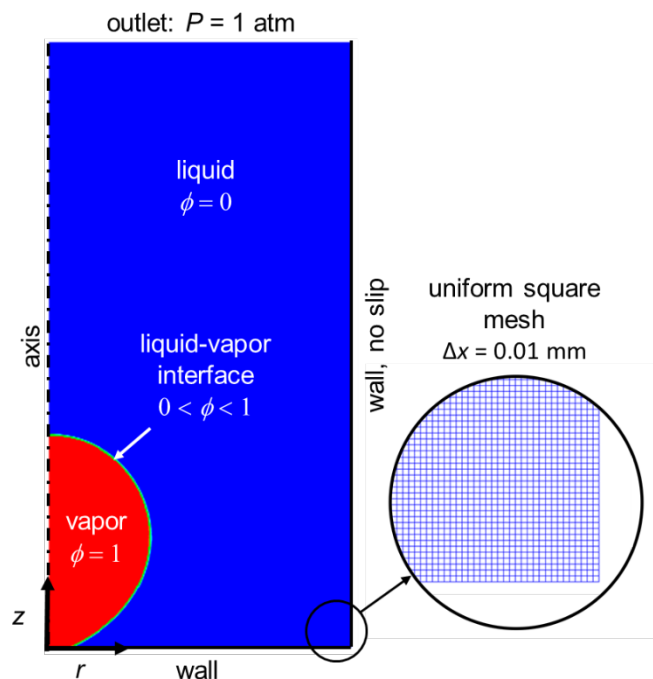


**Figure 3.** The rectangular, axisymmetric numerical simulation domain. The zoomed view shows the mesh geometry.

In the VOF simulations, the phases are tracked based on the volume fraction,  $\phi$ , within each individual cell. In this work, the phases are defined based upon the vapor volume fraction. As labeled in figure 3, liquid is present where  $\phi = 0$  (shown in blue) and vapor is present where  $\phi = 1$  (shown in red). The interface is found anywhere  $0 < \phi < 1$ . In the VOF solver, a single set of the Navier-Stokes equations incorporating the volume fraction is solved to determine the flow field. The interface is tracked using a geometric reconstruction interpolation scheme (Geo-Reconstruct). The volume fraction is used to determine the location of the contact line and the value of the contact angle for the duration of the simulation. The contact line is considered to be located at the cell adjacent to the bottom boundary with volume fraction closest to 0.5. The contact angle can be calculated based on the gradient of the volume fraction at the contact line as  $\theta = \cos^{-1}((\nabla\phi)_z / |\nabla\phi|)$  .. Both the contact line location and the contact angle are tracked throughout the simulation. A variable time step is implemented to ensure that the maximum Courant number remains less than 0.25, with a maximum time step of  $1 \times 10^{-6}$  s to mitigate the development of spurious currents.

The domain is initialized to be entirely liquid, except for an initial bubble. For each case, the bubble is initialized as a spherical cap at the receding contact angle where the radius of curvature is 0.3 mm. This provides a stable bubble with a sufficiently small contact radius to ensure that the maximum bubble radius and departure size are not influenced by the initial condition while remaining adequately resolved by the mesh. The bubble grows as a result of a user-defined mass source that is evenly distributed (volumetrically) across all vapor cells where  $\phi = 1$ . It is well known that inertia can play a dominant role in the bubble growth and departure process at high

growth rates. In this study, the goal is to characterize quasi-steady bubble growth independent of inertial effects. Oguz and Prosperetti<sup>42</sup> defined a critical volumetric growth rate for bubbles growing adiabatically from a needle, below which the departure size is independent of growth rate. It is adapted here based on the contact diameter rather than the needle diameter and is given as

$$Q_{cr} = \pi \left( \frac{16}{3g^2} \right)^{1/6} \left( \frac{\sigma D_c}{\rho_l} \right)^{5/6} . \quad (1)$$

The growth rate for the simulations is conservatively set to be 10% of the critical growth rate given by equation 1 in all cases, except those with both water as the working fluid and a 30 deg receding contact angle. In these cases, a constant growth rate of 50 mm<sup>3</sup>/s was used for numerical stability, which represents 8-12% of the critical growth rate.

The contact angle boundary condition and the contact line motion at the bottom boundary are controlled using a user-defined function (UDF). This UDF consists of two key components: a variable contact angle boundary condition and a contact line pinning mechanism. The contact angle boundary condition is native to ANSYS Fluent and sets the volume fraction gradient at the cell adjacent to the wall accordingly. To pin the contact line, a momentum source is applied at the contact line, similar to the approach used in the study of droplet impingement by Malgarinos *et al.*<sup>43</sup> The momentum source is analogous to a proportional-derivative controller and takes the form  $S_m = \pm k_1 (r_{CL} - r_{pin})^2 - k_2 \rho_{CL} \dot{r}_{CL}$ , where  $k_1$  and  $k_2$  are proportionality constants,  $r_{CL}$  is the radial position of the contact line,  $r_{pin}$  the location where the contact line should be pinned,  $\rho_{CL}$  the density of the cell that contains the contact line, and  $\dot{r}_{CL}$  the radial velocity of the contact line. The first term of the momentum source acts to push the contact line toward the pinned location based on the current distance between the contact line and the pinned location, with the sign set accordingly. The second term counteracts the current contact line velocity to minimize contact

line motion. To minimize instabilities, the momentum source is distributed throughout a total of six cells (the cells at and adjacent to the radial location of the contact line, within the two mesh rows closest to the surface). The constants  $k_1$  and  $k_2$  are tuned such that the contact line generally remains within one cell from the target pinning location during the simulations.

Implementation of the UDF simply ensures that the contact line is only able to recede if it is at the receding contact angle and advance at the advancing contact angle. In this way, the wetting dynamics are consistent with theory, but the proposed framework for bubble growth is not artificially forced. If the contact angle is less than or equal to the receding contact angle and the contact line is moving outward (dewetting), the contact angle boundary condition is set to the receding contact angle and no momentum source is applied. If the measured contact angle is greater than or equal to the advancing contact angle and the contact line is moving inward (wetting), the contact angle boundary condition is set to the advancing contact angle and no momentum source is applied. If either the contact angle or contact line motion does not satisfy these criteria, the contact line is pinned by applying the momentum source and the contact angle boundary condition is set to the measured contact angle at the end of each time step. For instance, if the contact angle is less than the receding contact angle but the contact line is moving toward the vapor, or the contact angle is between the advancing and receding contact angles, pinning is applied. The combination of the momentum source and reassigning of the contact angle boundary condition keeps the contact line pinned in place but allows the contact angle to change with each time step. For cases with no contact angle hysteresis,  $\theta_{adv} = \theta_{rec}$ , no pinning condition is applied, and the contact angle boundary condition remains constant throughout the simulation. This is the inherent assumption of using a single, static contact angle to describe contact line dynamics during boiling.

A wide range of dynamic contact angles (each inputs to the simulations) are evaluated for three different fluids, as summarized in table 1. Water, propane, and HFE-7100 were chosen due to their differences in capillary length ( $\lambda_c = \sqrt{\sigma / \Delta\rho g}$ ), which span a range typical of most fluids that would be considered for use in two-phase systems. The properties of each fluid used in the simulations are provided in table 2. The saturated fluid properties at a pressure of 1 atm were used for all fluids, with the exception of the viscosity. The viscosity generally does not play an important role in quasi-steady bubble dynamics<sup>2</sup>, but a low viscosity increases the susceptibility to spurious currents during numerical simulations<sup>44,45</sup>. For this reason, a fixed liquid viscosity value of  $\mu_l = 2.79 \times 10^{-3}$  N/m was used for all fluids, which is an order of magnitude larger than the saturation viscosity of water.

**Table 1.** Matrix of simulations performed where “W” indicates a simulation using water ( $\lambda_c = 2.5$  mm ), “P” propane ( $\lambda_c = 1.7$  mm ), and “H” HFE-7100 ( $\lambda_c = 0.9$  mm ).

		Advancing Contact Angle (deg)				
		30	60	90	120	150
Receding Contact Angle (deg)	30	W,P	W,P	W,P	W,P	W,P
	60	-	W,P,H	W,P,H	W,P,H	W,P,H
	90	-	-	W,P,H	W,P,H	W,P,H
	120	-	-	-	W,P,H	W
	140	-	-	-	-	W,P,H

**Table 2.** Fluid properties used during the simulations for each of the three fluids saturated at a pressure of 1 atm.

<b>Fluid</b>	<b>Liquid Density</b> ( $\rho_l$ , kg/m <sup>3</sup> )	<b>Vapor Density</b> ( $\rho_v$ , kg/m <sup>3</sup> )	<b>Surface Tension</b> ( $\sigma$ , N/m)	<b>Capillary Length</b> ( $\lambda_c$ , mm)
<b>Water</b>	957.9	0.6	0.0589	2.5
<b>Propane</b>	580.9	2.4	0.0158	0.9
<b>HFE-7100</b>	1370.2	9.9	0.0106	1.7

### 3. RESULTS AND DISCUSSION

A representative progression of the typical bubble growth as simulated with contact angle hysteresis is shown in figure 4 (water with  $\theta_{rec} = 30$  deg and  $\theta_{adv} = 120$  deg). Figure 4(a-b) show the temporal evolution of the contact radius and contact angle, respectively, during bubble growth with vertical lines dividing the stages of growth. Figure 4 (c-e) show the progression of bubble morphology within each of the growth stages. In the first stage of growth (receding, figure 4(c)), the bubble grows at the receding contact angle. The contact radius increases during this stage (figure 4(a)) as the surface dewets while the contact angle remains nearly constant (figure 4(b)). A maximum contact radius is reached at the start of the second stage of bubble growth (pinning, shown in figure 4(d)). The contact radius then remains constant as the contact line is pinned in place and the contact angle increases as the bubble grows. Eventually, the third stage (advancing, shown in figure 4(e)) commences once the contact angle reaches the advancing contact angle. The contact radius decreases rapidly as the surface rewets and the bubble quickly departs from the surface. There is not a pronounced constant contact angle mode during the advancing stage for this case because the stage lasts for such a short duration. The specific nature

of each of these stages varies depending on the dynamic contact angles and fluid properties, but the general behavior remains the same. In cases with no contact angle hysteresis, the pinning stage does not occur, and the contact angle is constant throughout the growth and departure process. For reference, the animations for all of the simulations using water are presented in movie S1.

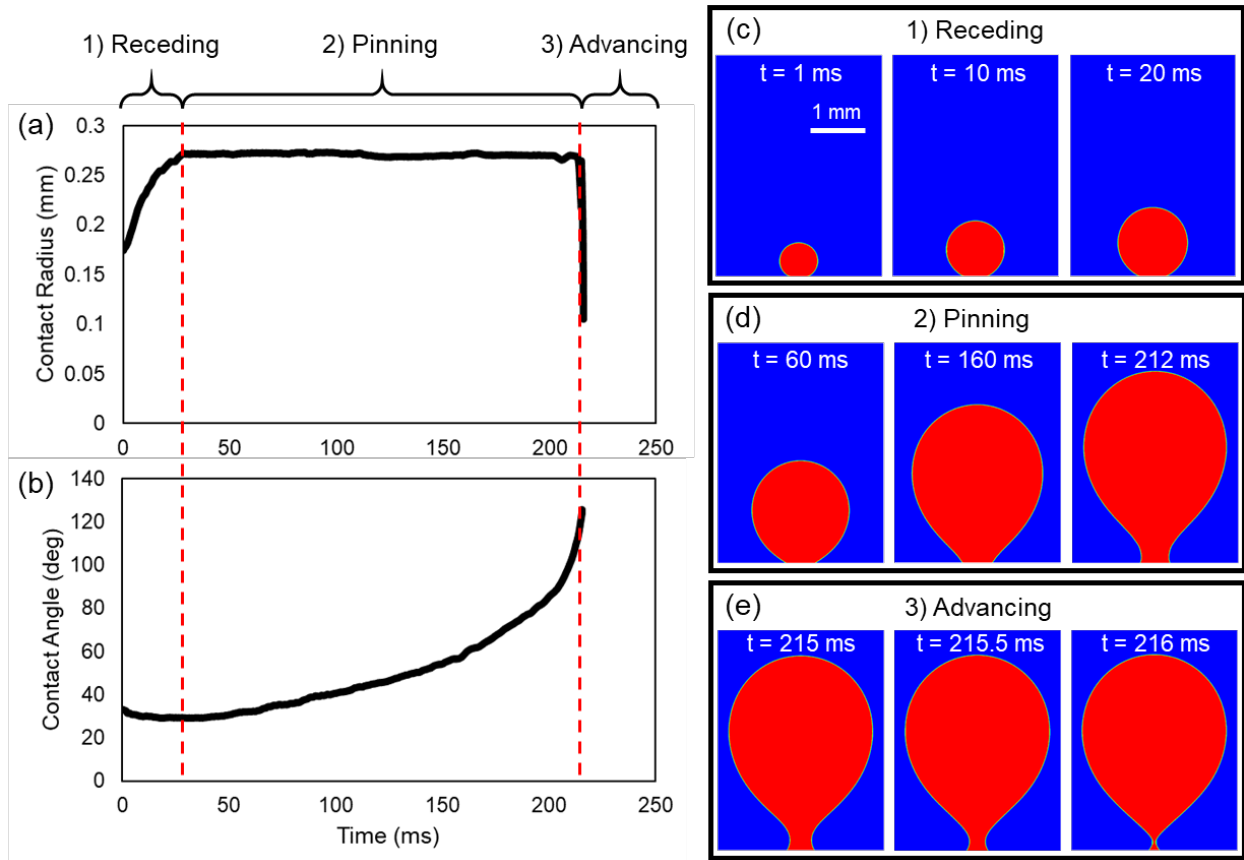


**Figure 4.** Simulated bubble growth and departure characteristics for water with  $\theta_{\text{rec}} = 30$  deg and  $\theta_{\text{adv}} = 120$  deg. Temporal evolution of (a) contact radius and (b) contact angle with vertical dashed lines dividing the annotated stages of growth. Phase contours showing the bubble morphologies during progression through the (c) receding, (d) pinning, and (e) advancing stages of growth.

### 3.1 The Role of Receding Contact Angle during Bubble Growth

According to the proposed framework, we theorize that the receding contact angle dictates the morphology of the bubble during the early stage of bubble growth because the contact line is receding as liquid dewets the surface. Therefore, the receding contact angle is expected to govern the maximum contact diameter, which occurs as the bubble transitions from the receding stage to the pinning mode. Figure 5 (a-c) shows the phase contours for bubbles as the maximum contact diameter is reached (*i.e.*, the transition between the receding and pinning stages) for receding contact angles of 30, 90, and 140 deg. Animations of all of the simulated cases with a 30 deg receding contact angle with water as the working fluid are presented in movie S2. For low receding contact angles, the contact diameter remains small as the bubble grows, as shown for  $\theta_{rec} = 30$  deg in figure 5(a). Thus, the surface tension forces act over a relatively short contact line length and the critical force balance (at which the contact angle must begin to increase to compensate for increasing buoyant forces) occurs at small bubble sizes, resulting in an early transition to the pinning mode and a small maximum contact diameter. As the receding contact angle increases, as demonstrated by the cases shown in figure 5(b,c), the bubble morphology changes such that the contact diameter becomes increasingly larger relative to the overall size of the bubble. The increased contact line length increases the overall surface tension force and requires a larger bubble volume to reach the critical balance between surface tension and buoyancy forces. As a result, the receding mode is prolonged, and the maximum contact diameter increases. With the dramatic increase in maximum contact diameter, the overall bubble volume at the point of transition to the pinning stage also increases substantially with increasing receding contact angle. Figure 5(d) shows the relative influence, or lack thereof, of the advancing and receding contact angles on the maximum contact diameter for water. The receding contact

angle has a dominant role; the maximum contact diameter changes by more than an order of magnitude when the receding contact angle is increased from 30 deg to 140 deg. The advancing contact angle, plotted along the abscissa, has no apparent influence on the contact diameter. For a given advancing contact angle, the maximum contact diameter remains constant even when the advancing contact angle is increased from 30 deg to 150 deg. *Because the receding contact angle governs the bubble morphology during the initial bubble growth stage prior to pinning of the contact line, it is the key surface wettability metric that determines the maximum contact diameter of a bubble.*

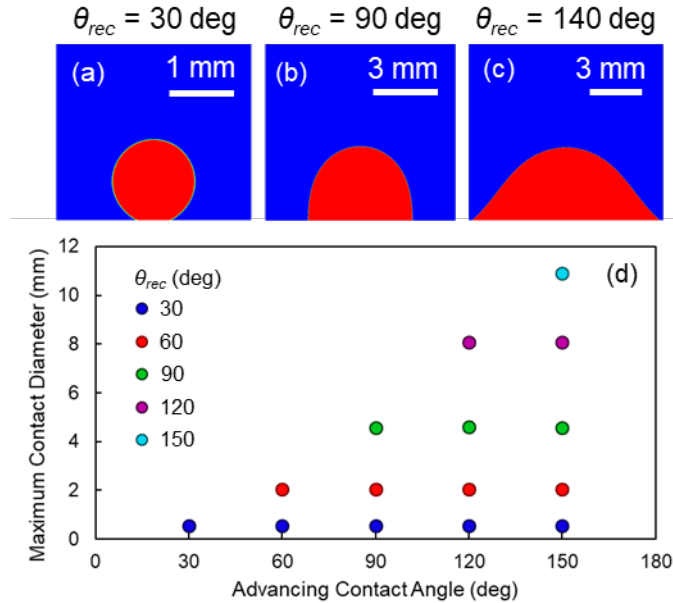


**Figure 5.** Phase contours of simulated water bubbles upon reaching the maximum contact diameter at the transition from the receding to the pinning stage of growth: (a)  $\theta_{rec} = 30$  deg, (b)  $\theta_{rec} = 90$  deg, and (c)  $\theta_{rec} = 140$  deg. Note that the scale bar in (a) differs from that of (b) and (c). (d) Maximum contact diameter plotted versus advancing contact angle for different receding contact angles for simulations of water bubble growth and departure.

### 3.2 The Role of Advancing Contact Angle during Bubble Departure

Following the proposed framework, we theorize that the advancing contact angle governs the bubble departure process as the liquid advances to rewet the surface. Effectively, the advancing contact angle acts as the threshold which dictates the end of the pinning stage at which point the contact line is allowed to advance. As a result, the bubble morphology during departure is determined by the advancing contact angle. Figure 6(a,b) show water bubble morphologies at the moment the contact line begins to advance for cases with the same receding contact angle ( $\theta_{\text{rec}} = 30 \text{ deg}$ ) and two different advancing contact angles ( $\theta_{\text{adv}} = 30 \text{ deg}, 90 \text{ deg}$ , respectively). For  $\theta_{\text{adv}} = 30 \text{ deg}$ , there is no contact angle hysteresis. Thus, there is no pinning stage and the bubble morphology is identical to that at the end of the receding stage shown in figure 5(a). The contact line is able to advance upon reaching the maximum contact diameter and the surface rewets as the bubble departs. As the advancing contact angle is increased to 90 deg, the contact line stays pinned after the receding stage until the contact angle increases to 90 deg. This keeps the bubble attached to the surface for a longer duration as the bubble continues to grow, resulting in an increased departure size. Because the contact diameter remains constant during the pinning stage of growth, the bubble morphology changes significantly and the region near the base begins to neck. If the advancing contact angle is increased further to 150 deg, as shown in figure 6(c), the bubble pinches off above the surface during the pinning stage before the advancing contact angle is reached, leaving a residual vapor bubble behind on the surface. This pinch-off mechanism, with or without advancement of the contact line, was observed in all simulations with  $\theta_{\text{adv}} > 90 \text{ deg}$  and has been observed in experiments on hydrophobic surfaces<sup>5,6,8</sup>. As a result of this phenomenon, bubbles will successively grow and depart at this same location with no waiting

time necessary for nucleation to occur. Side-by-side comparisons of animations of cases with differing advancing contact angles are presented in movie S1.

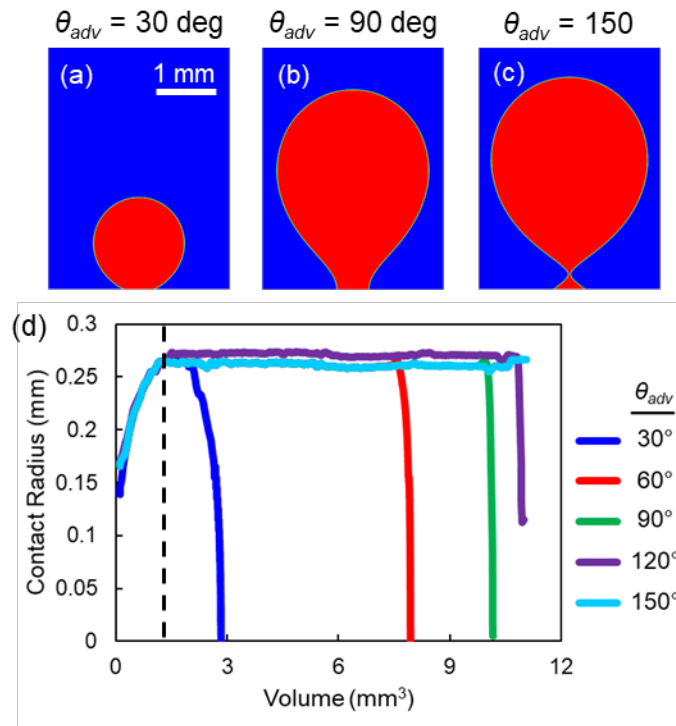


**Figure 6.** Phase contours showing the morphology of water bubbles at the moment when the contact line begins to advance for two advancing contact angles of (a) 30 deg and (b) 90 deg, and (c) the moment when pinch-off occurs for an advancing contact angle of 150 deg. (d) Bubble contact radius plotted versus bubble volume for water cases with a receding contact angle of 30 deg and a range of advancing contact angles. The black dashed line indicates the start of the pinning stage. For all cases shown, the receding contact angle is fixed to be 30 deg.

To illustrate the impact of advancing contact angle on the ebullition process, figure 6(d) shows the bubble contact radius plotted against the bubble volume for a constant receding contact angle ( $\theta_{rec} = 30$  deg) and multiple advancing contact angles ranging from 30 deg to 150 deg. For this constant receding contact angle, all five cases exhibit an identical trend of increasing bubble contact radius as the volume increases during the receding stage; as discussed

in Section 3.1, the advancing contact angle has no effect on the bubble morphology during this stage. After the maximum contact radius is reached, the duration of the pinning stage and the contact radius at which departure occurs differ between the cases. As the advancing contact angle increases, the duration of the pinning mode increases allowing the bubble to stay attached to the surface and grow larger before departure. Thus, an increased advancing contact angle leads to a larger departure volume. After the end of pinning, the contact radius reduces to zero during the advancing stage of growth for  $\theta_{adv} = 30, 60,$  and  $90$  deg as the bubble departs from the surface. This indicates that the bubble completely departs from the surface (*i.e.*, the surface fully rewets between departure events). For  $\theta_{adv} = 120$  deg, the contact line partially advances, but the bubble pinches off as the contact diameter approaches  $\sim 0.1$  mm, leaving behind a residual bubble. As mentioned previously, for  $\theta_{adv} = 150$  deg (figure 6(c)), the contact line does not have the opportunity to advance and the bubble pinches off at the maximum contact radius during the pinning stage. The advancing contact angle thus plays two key roles in bubble ebullition. *First, it determines the duration that the bubble spends in the pinning stage, affecting the final departure volume. Second, it determines the departure morphology, namely, whether the bubble fully departs from the surface or pinches off, leaving behind a residual bubble.*

### **3.3 Redefining Wettability Regimes Based on Dynamic Contact Angle**

With this understanding of the roles of advancing and receding contact angles, three fluid-property-independent classes of surface wettability can be defined in the context of boiling based upon the dynamic contact angles and the resulting qualitative bubble morphologies. For each classification, simulated results are compared directly against experimental observations on surfaces with characterized dynamic wetting behavior.

First, *hygrophilic* surfaces (where “hygro-” refers to any arbitrary liquid<sup>46</sup>) are defined as having both a low receding contact angle (less than 90 deg) and a low advancing contact angle (less than 90 deg). A bubble growth and departure simulation for a hygrophilic surface ( $\theta_{rec} = 30^\circ$ ,  $\theta_{adv} = 30^\circ$ ) is shown alongside experimental bubble visualizations for a smooth aluminum surface in figure 7. The aluminum surface was prepared and tested in a pool boiling facility as described in our prior work<sup>19</sup>. The static, receding, and advancing contact angles were measured to be 10 deg, <5 deg, and 29 deg, respectively. The simulation accurately replicates the progression of the bubble morphology observed experimentally. Boiling on hygrophilic surfaces is characterized by bubbles having relatively small contact diameters, owing to the low receding contact angle, which fully depart the surface without leaving behind any residual vapor due to the low advancing contact angle. Thus, our redefinition of hygrophilicity relies on the key bubble characteristics that result from the dynamic contact angles, rather than arbitrary correlation to the static contact angle. In this way, the terminology accurately represents the wetting dynamics and resulting bubble morphologies that are important to boiling.

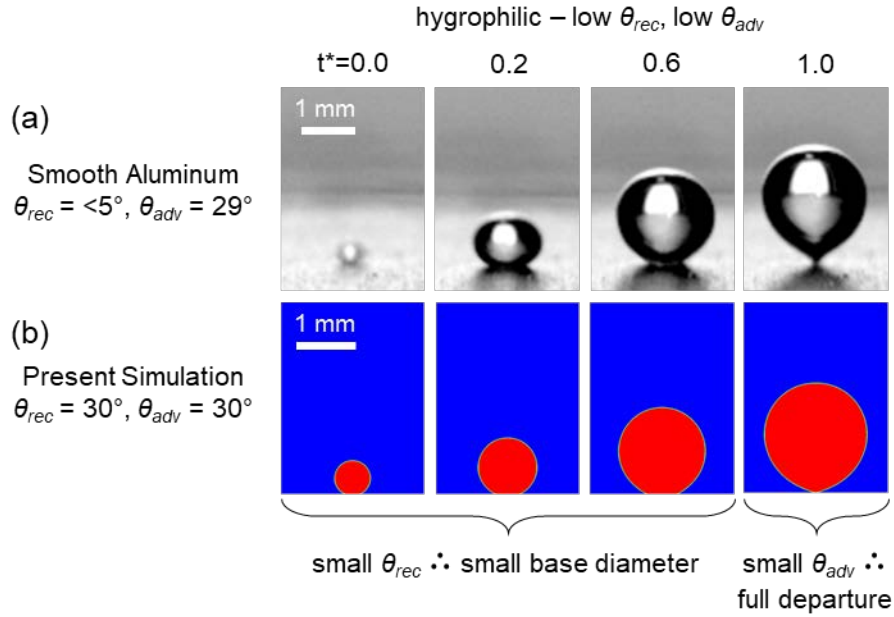


**Figure 7.** (a) Experimental images and (b) simulated phase contours for a progression of times, normalized by the departure time ( $t^* = t/t_{depart}$ ), showing the evolution of bubble morphology during growth and departure on a hydrophilic surface.

Similarly, *hydrophobic* surfaces can be defined for boiling as those having high receding contact angles (greater than 90 deg) and high advancing contact angles (greater than 90 deg). A bubble growth and departure simulation for a hydrophobic surface ( $\theta_{rec} = 120^\circ$ ,  $\theta_{adv} = 120^\circ$ ) is shown in figure 8 alongside our prior experimental visualization for a hydrophobic smooth Teflon surface<sup>8</sup>. Again, the simulations accurately capture the critical features of the bubble morphology when compared with the experimental results. Bubbles growing on hydrophobic surfaces have large contact diameters due to the large receding contact angle. The large advancing contact angle leads to the bubbles departing by pinching off above the surface, leaving behind a pocket of vapor which can immediately begin to grow, with no intervening waiting period for nucleation. As a result of these growth characteristics, specifically during the receding growth stage, vapor can readily spread along the surface and coalescence events can occur with

neighboring bubbles. This leads to large bubbles which can quickly cover an entire surface in boiling applications, resulting in premature film boiling<sup>4,6,8,19</sup>.

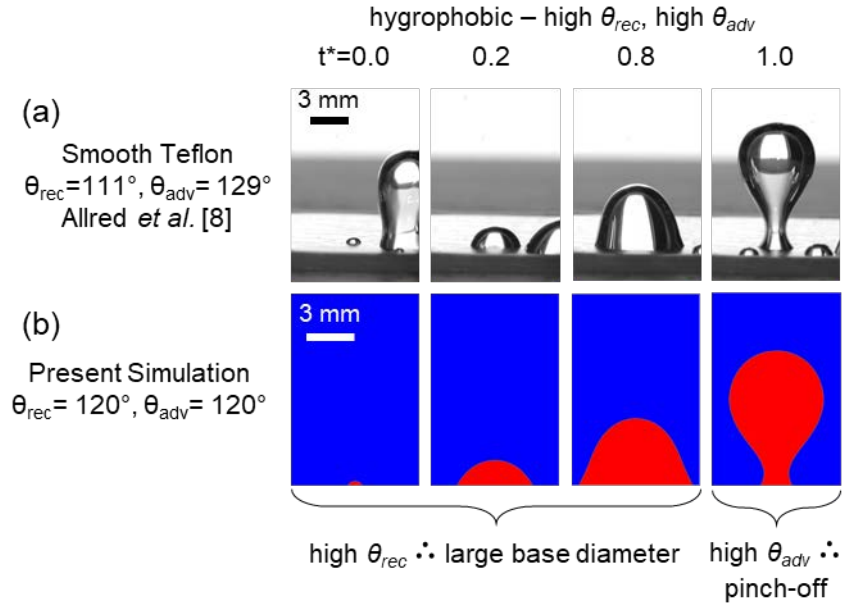


**Figure 8.** (a) Experimental images<sup>8</sup> and (b) simulated phase contours for a progression of times, normalized by the departure time ( $t^* = t/t_{depart}$ ), showing the evolution of bubble morphology during growth and departure on a hydrophobic surface.

Lastly, in the context of boiling, we define *ambiphilic* surfaces (“ambi-” referring to both liquid and vapor) as those having a low receding contact angle (less than 90 deg) but a high advancing contact angle (greater than 90 deg). These surfaces attract both the liquid (via low receding contact angle) and the vapor (via high advancing contact angle) of a given fluid. A bubble growth and departure simulation for an ambiphilic surface ( $\theta_{rec} = 30^\circ$ ,  $\theta_{adv} = 120^\circ$ ) is shown alongside experimental visualizations for an ambiphilic smooth PDMS surface ( $\theta_{rec} = 10^\circ$ ,  $\theta_{adv} = 110^\circ$ )<sup>8</sup> in figure 9. During boiling on ambiphilic surfaces, the low receding contact angle results in a small contact diameter as bubbles grow. The contact line then pins and the contact angle increases to a high advancing contact angle above 90 deg, such that the bubble necks and

pinches off, resulting in a residual vapor bubble left behind on the surface. As a result, ambiphilic surfaces exhibit favorable bubble dynamics: by minimizing vapor spreading over the surface similar to hydrophilic surfaces, but also eliminating the waiting time until the next bubble nucleates after departure similar to hydrophobic surfaces. A single static contact angle measurement cannot accurately portray an ambiphilic surface because the behavior results from contrasting receding and advancing contact angles. Animations comparing the experimentally observed and simulated bubble morphologies throughout the growth process on hydrophilic, hydrophobic, and ambiphilic surfaces are presented in movie S3.

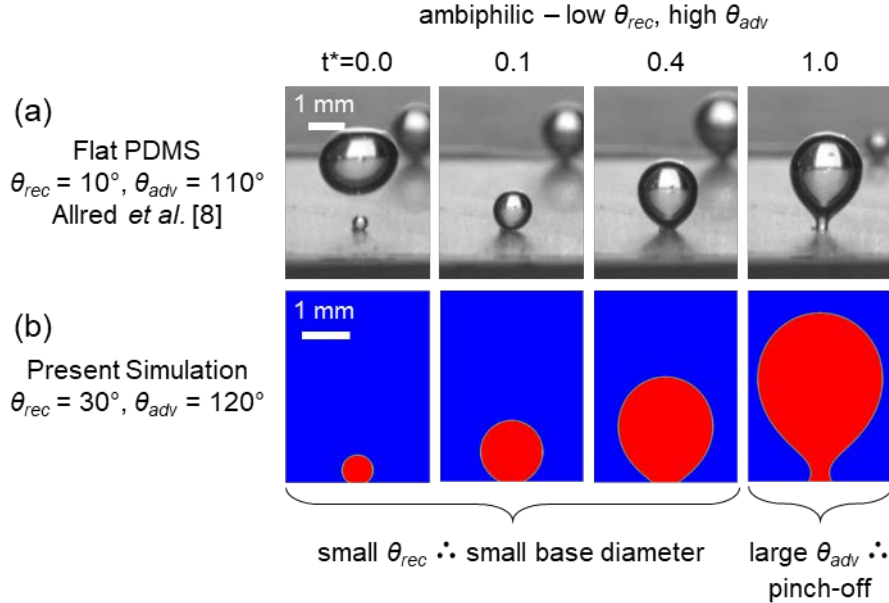


**Figure 9.** (a) Experimental images<sup>8</sup> and (b) simulation phase contours for a progression of times, normalized by the departure time ( $t^* = t/t_{depart}$ ), showing the evolution of bubble morphology during growth and departure on an ambiphilic surface. Scale bars are 1 mm.

Surfaces with extreme contact angle hysteresis, such as parahydrophobic<sup>8,47</sup> and superhydrophobic surfaces with liquid in the Wenzel state<sup>19</sup>, are likely to fall under this ambiphilic wettability classification. These surfaces are particularly poorly represented by a

static contact angle characterization making it critical to consider their dynamic wetting behavior. Because the contact line advances onto the surface during deposition of a sessile droplet, the static contact angle is usually closer to the advancing contact angle. Thus, these surfaces would commonly be (erroneously) classified as hydrophobic based on a static contact angle characterization<sup>8,19</sup>. However, in comparing the bubble morphologies shown in figure 8 and figure 9, the simulated and observed ebullition characteristics of amphiphilic surfaces are in stark contrast with those of hydrophobic surfaces. Additionally, these surfaces display favorable nucleation characteristics<sup>8,19</sup>, making them promising candidates for enhanced boiling surfaces.

### 3.4 Contact and Departure Diameter Models

In addition to defining these qualitative wettability classifications for boiling, the simulations provide quantitative data regarding the dependency of both maximum contact diameter and departure diameter on the dynamic contact angles. In order to determine a fluid-property-independent relationship between the dynamic contact angles and these parameters, the maximum contact diameter and departure diameter are nondimensionalized by dividing by the capillary length ( $\lambda_c = \sqrt{\sigma / (\rho_l - \rho_v) g}$ ). The bubble growth and departure processes are dominated by buoyant and surface tension forces. This nondimensionalization removes the influence of the fluid properties that affect buoyancy and surface tension, isolating the role of the bubble morphology, which is governed by the dynamic contact angles.

Figure 10 shows the relationship between the maximum contact diameter and the receding contact angle extracted from the simulation data. As previously demonstrated in Section 3.1, the advancing contact angle does not play a role in determining the maximum contact diameter, and therefore only the dependence on the receding contact angle is considered. Figure 10(a) shows

dimensional results for the three different fluids (water, propane, and HFE-7100). For each fluid, the trend of increasing contact diameter with increasing receding contact angle is observed, though the magnitudes of the contact diameters differ significantly. After nondimensionalizing, the normalized maximum contact diameters for the three fluids collapse neatly onto a single master curve.

Buoyant deformation of the bubble plays a significant role in determining the complex bubble shape. This makes it difficult to determine a relationship between bubble volume and contact diameter as the bubble grows. We are therefore precluded from making assumptions about the bubble geometry (*e.g.*, it is not a spherical cap) in order to develop a reduced-order analytical solution for the maximum contact diameter using a force balance between surface tension and buoyancy. Instead, a correlation is determined by fitting the nondimensionalized simulation data shown in figure 10(b)

$$\frac{D_c}{\lambda_c} = 2.28 \times 10^{-4} \theta_{rec}^2 . \quad (2)$$

This equation provides a novel correlation for the maximum base diameter based on the dynamic wetting behavior of a surface. A prediction of the maximum contact diameter is critical in the understanding of the wetting and coalescence dynamics during boiling.

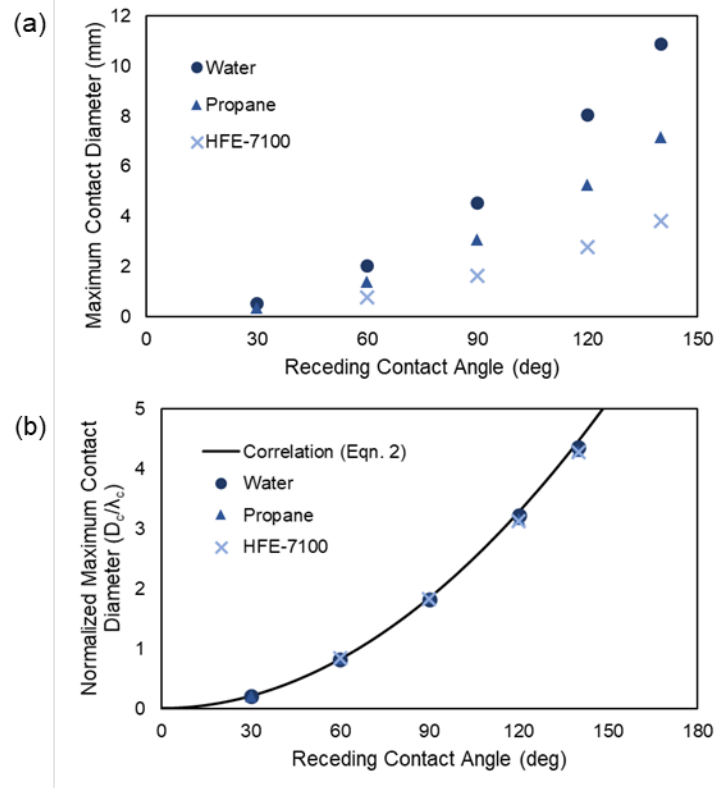


**Figure 10.** The maximum contact diameter, shown (a) dimensionally and (b) nondimensionalized by the capillary length, plotted versus receding contact angle for water, propane, and HFE-7100. In (b), the correlation presented in equation 2 is compared against the simulation results.

A bubble departure model is developed to determine the departure diameter based on the dynamic contact angles. In a simplified representation, the departure diameter can be approximated as the equivalent diameter of the bubble at which the buoyant force ( $F_b = \Delta\rho Vg$ ) balances the maximum vertical component of the surface tension force ( $F_s = \sigma\pi D_c \sin \theta$ ). The buoyant force monotonically increases as the bubble grows. On the other hand, the surface tension force can increase or decrease depending on the contact diameter and contact angle. As the bubble grows, the contact diameter and contact angle can change to counteract the increasing buoyancy within the constraints imposed by the dynamic contact angles. Thus, the surface

tension force threshold that the buoyant force must overcome for departure is the maximum surface tension force possible for a given set of dynamic contact angles. As established in the discussions above, the receding contact angle determines the maximum contact diameter, which corresponds to the maximum contact line length and thereby the highest surface tension force. Further, the vertical component of the surface tension is maximized when the contact angle approaches 90 deg. Because the advancing contact angle governs when the contact line will advance for bubble departure, it is considered to be the critical contact angle in this situation. Thus, if the advancing contact angle is less than or equal to 90 deg, the maximum possible surface tension force occurs at the maximum contact diameter and the advancing contact angle. After this condition is reached, departure is unhindered because the contact line will begin to advance and the contact line length will decrease, further reducing the surface tension force. If the advancing contact angle is greater than 90 deg, the maximum surface tension force occurs when the contact angle is 90 deg at the maximum contact diameter. After this point, the bubble begins to depart, but still must undergo morphological changes for the contact line to advance. Incorporating the correlation from equation 2 for the maximum contact diameter, this gives a piecewise relation for the departure diameter of a bubble based upon only the receding contact angle, the advancing contact angle, and the capillary length of the fluid

$$\frac{D_d}{\lambda_c} = \begin{cases} 0.111\theta_{rec}^{2/3} \sin^{1/3} \theta_{adv} & \text{if } \theta_{adv} < 90 \text{ deg} \\ 0.111\theta_{rec}^{2/3} & \text{if } \theta_{adv} > 90 \text{ deg} \end{cases} \quad (3)$$

Figure 11 shows the simulation results (symbols) and model predictions (lines) for the normalized departure diameter plotted against the advancing contact angle with different colored series representing different receding contact angles. The different shaded regions, from lightest to darkest, show the hydrophilic, amphiphilic, and hydrophobic regimes. The model from equation

3 accurately captures two key trends based upon the advancing and receding contact angles. First, at a fixed advancing contact angle, the departure diameter increases significantly with increasing receding contact angle. The increase in the receding contact angle leads to a larger contact diameter and higher surface tension force, keeping the bubble attached to the surface up to larger sizes. Second, for a fixed receding contact angle, there is a slight increase in the departure diameter as the advancing contact angle increases up to 90 deg, after which the departure diameter remains constant.

From the simulations, the departure diameter is considered to be the equivalent diameter based on the bubble volume just after the bubble pinches off or leaves the surface. The force balance model, which predicts departure to occur immediately when the buoyant force balances the maximum surface tension force, does not account for the time it takes for the bubble to rise and leave the surface. For low contact angles, this time is negligible and does not notably affect the departure size. However, for high contact angles, the bubble can grow significantly during this longer-duration process. For example, for a surface with a receding contact angle of 120 deg and an advancing contact angle of 150 deg for water, the bubble grows an additional 7% between the point at which the contact line begins to advance and the bubble fully departs from the surface. This is the reason that the force balance model underpredicts the departure diameter for hydrophobic surfaces with high advancing contact angles.

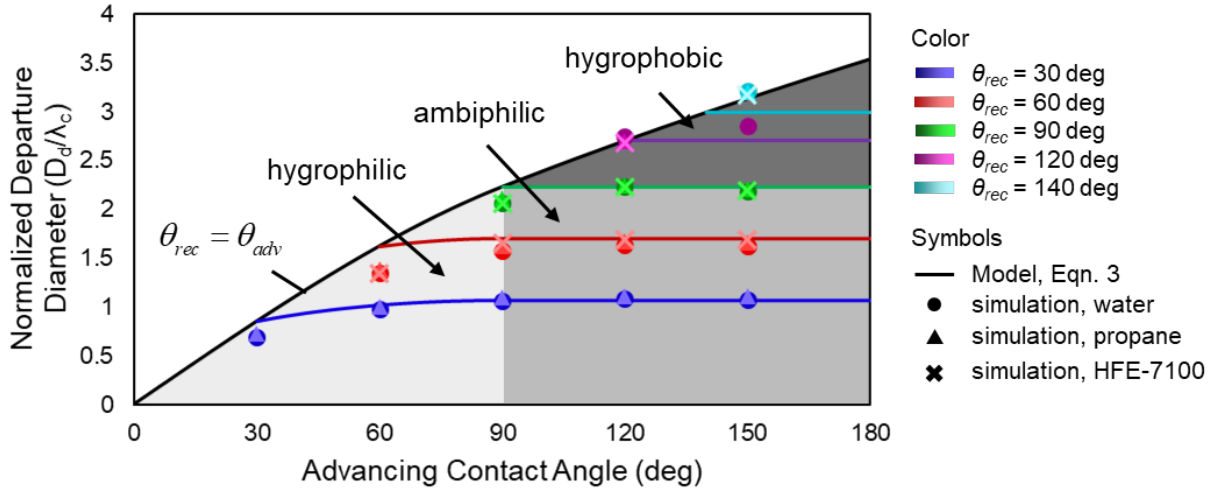


**Figure 11.** Simulation results and model predictions for the departure diameter, nondimensionalized by the capillary length, for water, propane, and HFE-7100 for a range of advancing and receding contact angles.

The predicted maximum contact diameter (equation 2) and departure diameter (equation 3) are compared with experiments<sup>5,7,8,48</sup> using water for a wide range of dynamic contact angles in figure 12. Each case in this bar chart is denoted by the receding (R##) and advancing (A##) contact angles at the bottom of the chart. The cases are organized as hydrophilic, amphiphilic, or hydrophobic, as indicated by the background shading matching that of figure 11. The wetting characteristics of each of the experimental surfaces are provided in table 3. From figure 12(a), it is observed that equation 2 accurately captures the experimental trends in maximum contact diameter with changes in the dynamic contact angle. However, the absolute contact diameter for cases with very low receding contact angle (~10 deg or less) are notably underpredicted. This is likely due to the quasi-steady nature of the simulations which ignores the inertia-controlled growth period commonly observed in the early stages of bubble growth<sup>49</sup>. It is speculated that the contact line expands to a larger diameter than the very small maximum contact diameter predicting using the quasi-steady assumption during this inertia-controlled stage of growth.

Figure 12(b) shows a comparison between the newly developed bubble departure diameter model (equation 3) and experimental measurements alongside the Fritz correlation<sup>12</sup>. The new model reduces the mean absolute error (MAE) in predicting the experimental departure diameter for these cases from 73% when computed using the Fritz correlation to 29% with equation 3. The greatest improvement is obtained for the ambiphilic surface with its substantial contact angle hysteresis. On this flat PDMS surface<sup>8</sup> (R10A110), the experimental departure diameter is reported as 2.3 mm. The Fritz correlation severely overpredicts a departure diameter of 7.8 mm (239% error) due to use of the static contact angle of 106 deg. Accounting for both the advancing and receding contact angles, the present model predicts a bubble departure diameter of 1.3 mm (43% error). Due to the aforementioned underprediction in the contact diameter for cases with very low receding contact angles, the experimental departure diameter is also underpredicted. Overall, the model developed here improves upon the existing standard for predicting departure diameter and accurately captures the relationship between surface wettability and bubble size.

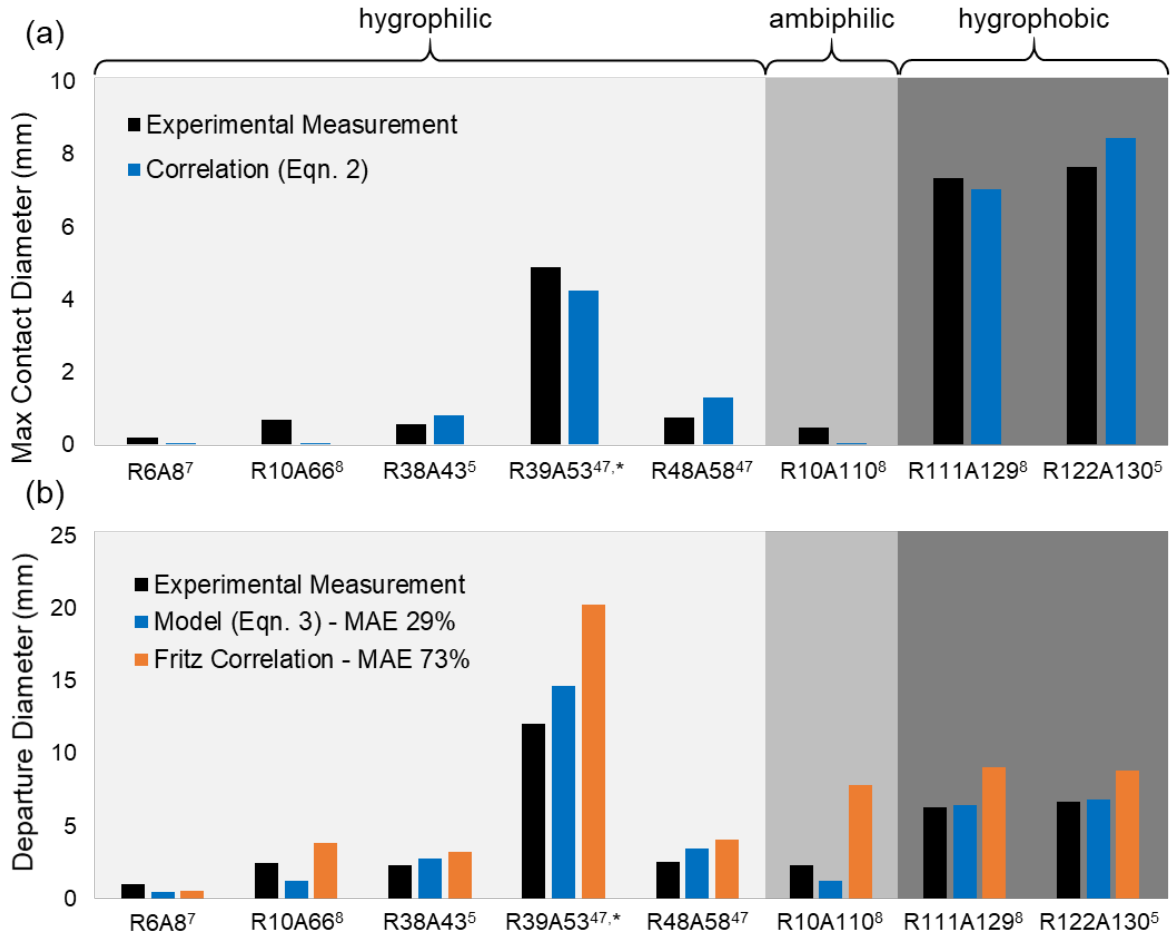


**Figure 12.** Comparisons between experimental results<sup>5,7,8,48</sup> and model predictions of the (a) maximum contact diameter and (b) departure diameter for bubble growth and departure during boiling. (\*The case “R39A53” is at reduced gravity,  $g' = 0.04g$  ).

**Table 3.** Measured contact angle values for the surfaces<sup>5,7,8,48</sup> compared in figure 12.

Label	$\theta_{rec}$ (deg)	$\theta_{adv}$ (deg)	$\theta_{static}$ (deg)	Reference
<b>R6A8</b>	6	8	8	Nam <i>et al.</i> <sup>7</sup>
<b>R10A66</b>	10	66	52	Allred <i>et al.</i> <sup>8</sup>
<b>R38A43</b>	38	43	44	Nam <i>et al.</i> <sup>5</sup>
<b>R39A53</b>	39	53	55	Qui <i>et al.</i> <sup>48</sup>
<b>(<math>g' = 0.04g</math>)</b>				
<b>R48A58</b>	48	58	55	Qui <i>et al.</i> <sup>48</sup>
<b>R10A110</b>	10	110	106	Allred <i>et al.</i> <sup>8</sup>
<b>R111A129</b>	111	129	123	Allred <i>et al.</i> <sup>8</sup>
<b>R122A130</b>	122	130	120	Nam <i>et al.</i> <sup>5</sup>

### 3.5 Implications and Limitations of the Study

The new understanding of the role of surface wettability during bubble growth and departure developed in this work suggests altering the design goals for surfaces in boiling applications. First, it is clear that the static contact angle is not an adequate predictor of the bubble dynamics during boiling. While it may provide a reasonable estimate for surfaces with very low contact angle hysteresis, static contact angle characterization risks dramatic overprediction of the departure size for surfaces with moderate-to-high contact angle hysteresis. Instead, the dynamic contact angles should be characterized for all boiling surfaces, as indicators of the bubble morphology and departure size, due to their role in the dewetting and rewetting processes throughout the ebullition cycle.

The wettability regimes of hydrophilic, hydrophobic, and amphiphilic, redefined based on the dynamic wetting behavior of the surface, provide a more complete understanding of how surfaces will behave in boiling applications. Hydrophilic surfaces minimize dewetting during bubble growth and readily rewet upon bubble departure. This results in small, rapidly departing bubbles and complete rewetting upon bubble departure. Hydrophobic surfaces both maximize dewetting during bubble growth and mitigate rewetting upon bubble departure. While they have exhibited potential advantages by offering high nucleation site densities and low boiling incipience temperatures, their dynamic wetting behavior leads to premature insulating vapor film coverage over the surface and precludes their use in most boiling applications<sup>4-6,8,15</sup>. The unique bubble dynamics of amphiphilic surfaces are clearly revealed in this study. Amphiphilic surfaces produce small bubbles that pinch off above the surface upon departure. The majority of the surface remains wetted, explaining the observed critical heat flux values on par with those of hydrophilic surfaces<sup>8,19</sup>. However, amphiphilic surfaces are also reported to exhibit higher heat transfer

coefficients than hydrophilic surfaces<sup>8,19</sup>. Based on the minimal rewetting on these surfaces owing to the high advancing contact angles, it is expected that they trap vapor within cavities on the surface very easily, replicating the favorable nucleation characteristics of hydrophobic surfaces. Additionally, the pinch-off departure mechanism completely eliminates the waiting time between the growth of successive bubbles and may result in more efficient heat transfer. These findings call for development of amphiphilic surfaces for boiling applications for a variety of fluids.

While the model proposed herein captures the contact line and contact angle dynamics across a wide range of dynamic wetting behaviors, it does have limitations based on the model assumptions. First, as discussed in the sections above, the quasi-steady assumption may not be valid for all situations during boiling, particularly for low receding contact angles. The growth rate of a bubble is highly dependent on the surface superheat during boiling<sup>49</sup> and can be influenced by the presence of a microlayer. Based on the analysis by Oguz and Prosperetti<sup>42</sup>, the growth rate threshold under which the quasi-steady assumption is valid is expected to scale with the contact diameter. Thus, surfaces with low receding contact angles are more prone to inertia-dominated growth and the effect will increase with higher surface superheats. Additional studies on the contact line and contact angle dynamics during inertia-controlled growth would provide a pathway for improved accuracy at low receding contact angles. Second, this model considers an adiabatic analysis based purely on wetting dynamics. Thus, contact line evaporation, which may have an influence on the maximum contact diameter over time, is ignored. Convective currents which may influence the force balance acting on the bubble are also neglected. Despite these simplifications, the newly developed models for the maximum contact diameter and departure diameter provide more accurate estimates of these parameters for most surfaces due to their consideration of the full spectrum of dynamic wetting behavior.

#### 4. CONCLUSIONS

This study introduces a theoretical framework for the contact line and contact angle evolution during bubble growth that is based on wetting dynamics. The bubble growth process is divided into three stages: receding, pinning, and advancing. The bubble initially grows as the liquid dewets the surface at the receding contact angle, followed by contact line pinning as the contact angle increases from the receding contact angle to the advancing contact angle; finally, the liquid rewets the surface at the advancing contact angle as the bubble departs. Numerical simulations of bubble growth and departure are performed based on this framework to investigate the effect of varying dynamic surface wettability on the ebullition characteristics. The receding contact angle solely determines the maximum contact diameter during bubble growth. The receding contact angle is also the dominant wetting characteristic that dictates the departure diameter, but the advancing contact angle also plays a lesser role. In general, lower dynamic contact angles result in smaller contact diameters and departure diameters. These findings reinforce the assertion that dynamic contact angles, rather than the static contact angle, should be considered when characterizing boiling surfaces. For boiling applications, the hydrophilic and hydrophobic wetting regimes are redefined based on the dynamic contact angles rather than a single static contact angle. Additionally, a new class of amphiphilic boiling surfaces is defined as having receding contact angles less than 90 deg and advancing contact angles greater than 90 deg. These surfaces display unique bubble dynamics that combine salutary elements from hydrophilic and hydrophobic surfaces and warrant further investigation. Models for the maximum base diameter and departure diameter of a bubble are developed requiring inputs of only the dynamic contact angles and the fluid properties. By accounting for the dynamic contact angles, the predictive

accuracy for departure diameter is significantly improved compared with the widely used Fritz correlation.

## **ASSOCIATED CONTENT**

### **Supporting Information**

Movie S1. Animations showing the bubble growth and departure process for all of the simulation cases performed using water as the fluid.

Movie S2. Animations showing the evolution of the morphology during bubble growth on surfaces with differing receding contact angles.

Movie S3. Animations comparing the experimentally observed and simulated bubble morphologies on hydrophilic, hydrophobic, and amphiphilic surfaces.

## **AUTHOR INFORMATION**

### **Corresponding Author**

\*E-mail: [sureshg@purdue.edu](mailto:sureshg@purdue.edu)

### **Notes**

The authors declare no competing financial interest.

## ACKNOWLEDGEMENTS

The authors thank the Office of Naval Research (ONR) Naval Enterprise Partnership Teaming with Universities for National Excellence (NEPTUNE) program for financial support of this work under grant number N00014-15-1-2833.

The first author acknowledges support from the Department of Defense (DoD) National Defense Science and Engineering Graduate Fellowship (NDSEG) program, sponsored by the Air Force Office of Scientific Research (AFOSR).

## REFERENCES

- (1) Prosperetti, A.; Lezzi, A. Bubble Dynamics in a Compressible Liquid. Part 1. First-Order Theory. *J. Fluid Mech.* 1986, 168, 457–478.
- (2) Mohanty, R. L.; Das, M. K. A Critical Review on Bubble Dynamics Parameters Influencing Boiling Heat Transfer. *Renew. Sustain. Energy Rev.* 2017, 78, 466–494.
- (3) Cavanagh, D. P.; Eckmann, D. M. Interfacial Dynamics of Stationary Gas Bubbles in Flows in Inclined Tubes. *J. Fluid Mech.* 1999, 398, 225–244.
- (4) Takata, Y.; Hidaka, S.; Uraguchi, T. Boiling Feature on a Super Water-Repellent Surface. *Heat Transf. Eng.* 2006, 27 (8), 25–30.
- (5) Nam, Y.; Wu, J.; Warrior, G.; Ju, Y. S. Experimental and Numerical Study of Single Bubble Dynamics on a Hydrophobic Surface. *J. Heat Transf.* 2009, 131 (12), 121004–121004.
- (6) Jo, H.; Ahn, H. S.; Kang, S.; Kim, M. H. A Study of Nucleate Boiling Heat Transfer on Hydrophilic, Hydrophobic and Heterogeneous Wetting Surfaces. *Int. J. Heat Mass Transf.* 2011, 54 (25–26), 5643–5652.
- (7) Nam, Y.; Aktinol, E.; Dhir, V. K.; Ju, Y. S. Single Bubble Dynamics on a Superhydrophilic Surface with Artificial Nucleation Sites. *Int. J. Heat Mass Transf.* 2011, 54 (7–8), 1572–1577.
- (8) Allred, T. P.; Weibel, J. A.; Garimella, S. V. The Petal Effect of Parahydrophobic Surfaces Offers Low Receding Contact Angles That Promote Effective Boiling. *Int. J. Heat Mass Transf.* 2019, 135, 403–412.

- (9) Gennes, P.-G. de; Brochard-Wyart, F.; Quere, D. *Capillarity and Wetting Phenomena: Drops, Bubbles, Pearls, Waves*; Springer-Verlag: New York, 2004.
- (10) Young, T. *An Essay on the Cohesion of Fluids*. *Philos. Trans. R. Soc. Lond.* 1805, 95, 65–87.
- (11) Dussan, E. B. *On the Spreading of Liquids on Solid Surfaces: Static and Dynamic Contact Lines*. *Annu. Rev. Fluid Mech.* 1979, 11 (1), 371–400.
- (12) Fritz, W. *Maximum Volume of Vapor Bubbles*. *Phys. Z.* 1935, 36, 379–384.
- (13) Wang, C. H.; Dhir, V. K. *Effect of Surface Wettability on Active Nucleation Site Density During Pool Boiling of Water on a Vertical Surface*. *J. Heat Transf.* 1993, 115 (3), 659–669.
- (14) Takata, Y.; Hidaka, S.; Cao, J. M.; Nakamura, T.; Yamamoto, H.; Masuda, M.; Ito, T. *Effect of Surface Wettability on Boiling and Evaporation*. *Energy* 2005, 30 (2–4), 209–220.
- (15) Betz, A. R.; Xu, J.; Qiu, H.; Attinger, D. *Do Surfaces with Mixed Hydrophilic and Hydrophobic Areas Enhance Pool Boiling?* *Appl. Phys. Lett.* 2010, 97 (14), 141909.
- (16) Hsu, C.-C.; Chen, P.-H. *Surface Wettability Effects on Critical Heat Flux of Boiling Heat Transfer Using Nanoparticle Coatings*. *Int. J. Heat Mass Transf.* 2012, 55 (13–14), 3713–3719.
- (17) Gong, S.; Cheng, P. *Lattice Boltzmann Simulations for Surface Wettability Effects in Saturated Pool Boiling Heat Transfer*. *Int. J. Heat Mass Transf.* 2015, 85, 635–646.
- (18) Frankiewicz, C.; Attinger, D. *On Temporal Biphilicity: Definition, Relevance, and Technical Implementation in Boiling Heat Transfer*. *J. Heat Transf.* 2017, 139 (11), 111511–111514.
- (19) Allred, T. P.; Weibel, J. A.; Garimella, S. V. *Enabling Highly Effective Boiling from Superhydrophobic Surfaces*. *Phys. Rev. Lett.* 2018, 120 (17), 174501.
- (20) Cassie, A. B. D.; Baxter, S. *Wettability of Porous Surfaces*. *Trans. Faraday Soc.* 1944, 40 (0), 546–551.
- (21) Patankar, N. A. *Transition between Superhydrophobic States on Rough Surfaces*. *Langmuir* 2004, 20 (17), 7097–7102.
- (22) Lafuma, A.; Quéré, D. *Superhydrophobic States*. *Nat. Mater.* 2003, 2 (7), 457–460.
- (23) Wier, K. A.; McCarthy, T. J. *Condensation on Ultrahydrophobic Surfaces and Its Effect on Droplet Mobility: Ultrahydrophobic Surfaces Are Not Always Water Repellent*. *Langmuir* 2006, 22 (6), 2433–2436.

- (24) Chen, C.-H.; Cai, Q.; Tsai, C.; Chen, C.-L.; Xiong, G.; Yu, Y.; Ren, Z. Dropwise Condensation on Superhydrophobic Surfaces with Two-Tier Roughness. *Appl. Phys. Lett.* 2007, 90 (17), 173108.
- (25) Chen, X.; Wu, J.; Ma, R.; Hua, M.; Koratkar, N.; Yao, S.; Wang, Z. Nanograsped Micropyramidal Architectures for Continuous Dropwise Condensation. *Adv. Funct. Mater.* 2011, 21 (24), 4617–4623.
- (26) Enright, R.; Miljkovic, N.; Al-Obeidi, A.; Thompson, C. V.; Wang, E. N. Condensation on Superhydrophobic Surfaces: The Role of Local Energy Barriers and Structure Length Scale. *Langmuir* 2012, 28 (40), 14424–14432.
- (27) Wu, A.; Vahabi, H.; Cha, H.; Chavan, S.; Kota, A. K. Dropwise Condensation on Hydrophilic Surfaces, The 10<sup>th</sup> International Conference on Boiling & Condensation Heat Transfer. Nagasaki, Japan, 2018.
- (28) Picknett, R. G.; Bexon, R. The Evaporation of Sessile or Pendant Drops in Still Air. *J. Colloid Interface Sci.* 1977, 61 (2), 336–350.
- (29) Kulinich, S. A.; Farzaneh, M. Effect of Contact Angle Hysteresis on Water Droplet Evaporation from Super-Hydrophobic Surfaces. *Appl. Surf. Sci.* 2009, 255 (7), 4056–4060.
- (30) Kunkelmann, C.; Ibrahim, K.; Schweizer, N.; Herbert, S.; Stephan, P.; Gambaryan-Roisman, T. The Effect of Three-Phase Contact Line Speed on Local Evaporative Heat Transfer: Experimental and Numerical Investigations. *Int. J. Heat Mass Transf.* 2012, 55 (7–8), 1896–1904.
- (31) Wang, F.-C.; Wu, H.-A. Pinning and Depinning Mechanism of the Contact Line during Evaporation of Nano-Droplets Sessile on Textured Surfaces. *Soft Matter* 2013, 9 (24), 5703–5709.
- (32) Dash, S.; Garimella, S. V. Droplet Evaporation Dynamics on a Superhydrophobic Surface with Negligible Hysteresis. *Langmuir* 2013, 29 (34), 10785–10795.
- (33) Phan, H. T.; Caney, N.; Marty, P.; Colasson, S.; Gavillet, J. Surface Wettability Control by Nanocoating: The Effects on Pool Boiling Heat Transfer and Nucleation Mechanism. *Int. J. Heat Mass Transf.* 2009, 52 (23–24), 5459–5471.
- (34) Jo, H.; Park, H. S.; Kim, M. H. Single Bubble Dynamics on Hydrophobic–Hydrophilic Mixed Surfaces. *Int. J. Heat Mass Transf.* 2016, 93, 554–565.
- (35) Kim, S. H.; Lee, G. C.; Kang, J. Y.; Moriyama, K.; Park, H. S.; Kim, M. H. The Role of Surface Energy in Heterogeneous Bubble Growth on Ideal Surface. *Int. J. Heat Mass Transf.* 2017, 108, Part B, 1901–1909.

- (36) Wang, X.; Wu, Z.; Wei, J.; Sundén, B. Correlations for Prediction of the Bubble Departure Radius on Smooth Flat Surface during Nucleate Pool Boiling. *Int. J. Heat Mass Transf.* 2019, 132, 699–714.
- (37) Mukherjee, A.; Kandlikar, S. G. Numerical Study of Single Bubbles with Dynamic Contact Angle during Nucleate Pool Boiling. *Int. J. Heat Mass Transf.* 2007, 50 (1), 127–138.
- (38) Chen, Y.; Mertz, R.; Kulenovic, R. Numerical Simulation of Bubble Formation on Orifice Plates with a Moving Contact Line. *Int. J. Multiph. Flow* 2009, 35 (1), 66–77.
- (39) Shikhmurzaev, Y. D. The Moving Contact Line on a Smooth Solid Surface. *Int. J. Multiph. Flow* 1993, 19 (4), 589–610.
- (40) Fluent, ANSYS Fluent 19.2, ANSYS-Fluent Inc., Canonsburg, PA.
- (41) Oguz, H. N.; Prosperetti, A. Dynamics of Bubble Growth and Detachment from a Needle. *J. Fluid Mech.* 1993, 257, 111–145.
- (42) Malgarinos, I.; Nikolopoulos, N.; Marengo, M.; Antonini, C.; Gavaises, M. VOF Simulations of the Contact Angle Dynamics during the Drop Spreading: Standard Models and a New Wetting Force Model. *Adv. Colloid Interface Sci.* 2014, 212, 1–20.
- (43) Galusinski, C.; Vigneaux, P. On Stability Condition for Bifluid Flows with Surface Tension: Application to Microfluidics. *J. Comput. Phys.* 2008, 227 (12), 6140–6164.
- (44) Deshpande, S. S.; Anumolu, L.; Trujillo, M. F. Evaluating the Performance of the Two-Phase Flow Solver InterFoam. *Comput. Sci. Discov.* 2012, 5 (1), 014016.
- (45) Marmur, A. From Hydrophilic to Superhydrophobic: Theoretical Conditions for Making High-Contact-Angle Surfaces from Low-Contact-Angle Materials. *Langmuir* 2008, 24 (14), 7573–7579.
- (46) Szczepanski, C. R.; Guittard, F.; Darmanin, T. Recent Advances in the Study and Design of Parahydrophobic Surfaces: From Natural Examples to Synthetic Approaches. *Adv. Colloid Interface Sci.* 2017, 241, 37–61.
- (47) Qiu, D. M.; Dhir, V. K.; Chao, D.; Hasan, M. M.; Neumann, E.; Yee, G.; Birchenough, A. Single-Bubble Dynamics During Pool Boiling Under Low Gravity Conditions. *J. Thermophys. Heat Transf.* 2002, 16 (3), 336–345.
- (48) Carey, V. P. *Liquid Vapor Phase Change Phenomena: An Introduction to the Thermophysics of Vaporization and Condensation Processes in Heat Transfer Equipment*, Second Edition, 2nd ed.; Taylor & Francis, 2008.

